Graphitization of Glassy Carbon after Compression at Room Temperature

T. B. Shiell, D. G. McCulloch, D. R. McKenzie, M. R. Field, B. Haberl, R. Boehler, B. A. Cook, C. de Tomas, I. Suarez-Martinez, N. A. Marks, and J. E. Bradby

Graphitization of Glassy Carbon after Compression at Room Temperature

T. B. Shiell[1]*, D.G. McCulloch[2,3], D.R. McKenzie[4], M.R. Field[3], B. Haberl[5], R. Boehler[5,6], B.A. Cook[2], C. de Tomas[7], I. Suarez-Martinez[7], N. A. Marks[7] and J. E. Bradby[1]

[1]Department of Electronic Materials Engineering, Research School of Physics and Engineering, The Australian National University, Canberra, ACT 2601, Australia
[2]Physics, School of Science, RMIT University, Melbourne, VIC 3001, Australia
[3]RMIT Microscopy & Microanalysis Facility, RMIT University, Melbourne, VIC 3001, Australia
[4]School of Physics, The University of Sydney, NSW 2006, Australia
[5]Neutron Scattering Division, Neutron Sciences Directorate, Oak Ridge National Laboratory, Oak Ridge, TN 37831, USA
[6]Geophysical Laboratory, Carnegie Institution of Washington, 5251 Branch Rd, NW Washington, DC 20015, USA
[7]Department of Physics and Astronomy, Curtin University, Perth, WA 6845, Australia

*Corresponding author email: tom.shiell@anu.edu.au

Glassy carbon is a technologically important material with isotropic properties that is non-graphitizing up to ~3000°C and displays complete or 'superelastic' recovery from large compression. The pressure limit of these properties is not yet known. Here we use experiments and modelling to show permanent densification and preferred orientation occurs in glassy carbon loaded to 45 GPa and above, where 45 GPa represents the limit to the superelastic and non-graphitizing properties of the material. The changes are explained by a transformation from its sp^2 rich starting structure to a sp^3 rich phase that reverts to fully sp^2 bonded oriented graphite during pressure release.

The flexibility of the carbon atom in forming covalent bonds with different hybridisation states leads to carbon solids which exhibit a range of useful properties from the extreme hardness of diamond to the extreme 'slipperiness' of graphite [1-3]. Glassy carbon (GC) is a predominately sp^2 bonded carbon which has exceptional 'superelastic' mechanical properties in which it completely recovers its shape after large compressive strains [4]. The material is a non-crystalline solid which is formed by the high temperature decomposition of cross-linked polymers [5]. GC has a low macroscopic density (~1.5 g/cc) when compared to graphite (2.27 g/cc) and is by definition a non-graphitizing carbon (i.e. it resists the development of graphite crystals) even when heated to temperatures up to 3000°C [6,7]. It is superior to graphite for applications such as non-contaminating crucibles and electrodes in electrochemical devices. GC is also being investigated for use in tribological applications including medical prosthetics [8] and wear resistant surfaces under extreme conditions (e.g. aircraft brakes) [9,10]. Transmission electron microscope (TEM) images reveal that GC has a characteristic nanostructure that has been interpreted as either a tangle of graphitic ribbons [5], or an assemblage of sheet-like structures containing fullerene-like elements [11]. Its novel nanostructure also makes it a useful precursor material for the synthesis of new carbon polymorphs such as nanocrystalline hexagonal diamond [12].

The structural origin of the resistance of GC to graphitization remains a topic of discussion in the literature [5,13,14]. GC can be also classified into two 'types', where Type 1 has a heat treatment temperature less than 2000ºC, and Type 2 has a heat treatment temperature greater than 2000ºC. Only subtle differences in the high pressure behavior between the two types have been reported [15]. Some authors have proposed that GC contains a small fraction of sp^3 bonds which act as cross-links between graphitic sheets or ribbons [11]. The structural origin of the superelastic property also remains unknown. Some authors propose that it is associated with a shape memory effect embodied within the sheet-like nanostructure [4,15] with the graphene sheet as a structural element retaining the memory of its initial shape. When compressed, the sheets develop some bonding interactions that do not change the original topology of the sheets, enabling the structure to return to its original configuration after decompression. Any sp^3 bonds acting as cross-links in GC contribute to this superelastic behaviour, governing the time response of the shape recovery.

Some high pressure studies have been used to show that GC undergoes a reversible bonding transformation from sp^2 rich to sp^3 rich at pressures beyond 40 GPa at room temperature [16], while other work reports that a substantial content of sp^2 bonding remains while the material is held under pressures of up to 60 GPa [17]. It has also been reported that GC becomes transparent when compressed above 33 GPa [18], suggesting that the majority of the material becomes sp^3 bonded. Another study found a permanent increase in macroscopic density of 10% following compression to 35 GPa [15]. However, none of the room temperature, high pressure studies of GC provide clear evidence of sp^3 bonds in the recovered samples at ambient pressure. Several simulations do show that compressing graphitic materials induces the formation of sp^3 bonding, leading to many different hybrid sp^2/sp^3 structures with diamond-like densities, but only while the pressure is maintained [19-23]. Above room temperature the high pressure results are different again. Recent reports have shown hexagonal diamond formed at 400°C [12], increased sp^3 bonding by heating up to 1200°C [24], and the recovery of a highly disordered, almost 100% sp^3 bonded material after laser heating [25].

An unanswered question regarding the high pressure behaviour of GC is the maximum pressure to which GC can be subjected before it loses its distinctive non-graphite like properties and isotropic tangled sheet-like nanostructure. This question is of direct relevance to tribological performance of GC since the pressure threshold determines how much of a GC wear surface is converted to a graphitic structure with the remainder retained as a superplastic 3-D network solid. In this study, we address this question by subjecting GC to compression in diamond anvil cells (DACs) and characterizing the recovered samples using Raman spectroscopy and TEM. To assist in the interpretation of the experiments the compression and decompression processes are simulated using molecular dynamics.

The GC sample used in this work has a macroscopic density of 1.42 g/cc and was purchased in the form of a solid plate from Hochtemperatur Werkstoffe (Sigradur-G). It was manufactured from a phenolic resin heated to 3000°C. Small chips (~80x80x50 µm) were loaded without a pressure medium into a Boehler Almax plate-DAC and raised to maximum pressures of 4, 10, 25, 35, 45, and 54 GPa using diamonds with 400 µm diameter culets. The absence of a pressure medium results in a significant uniaxial component in the supplied stress field. For all experiments, stainless-steel gaskets were used with sample chambers initially 200 µm in diameter and 55 µm deep. Pressures were determined *in situ* by the shift of the R1-ruby fluorescence line and the shift of the main diamond Raman peak in the centre of the gasket hole [26]. Figure 1 shows a schematic of the experimental procedure for preparing TEM specimens which involved using a focussed ion beam (FEI Scios Dualbeam) to retrieve samples of GC following compression in a DAC.
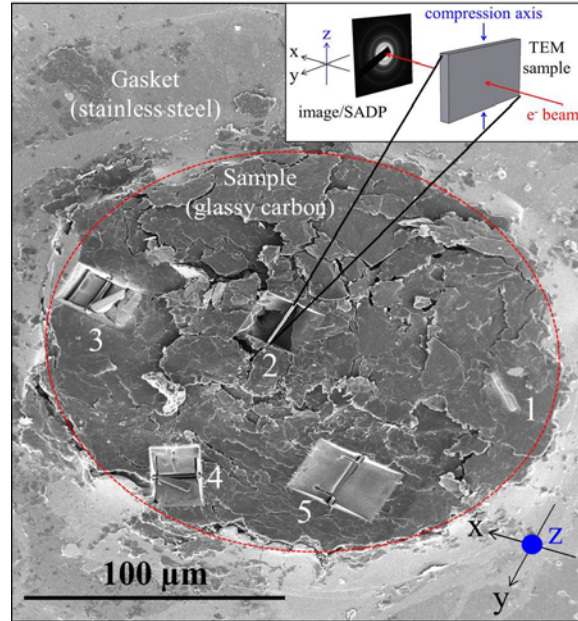
Figure 1: An SEM image of a GC sample after recovery from the DAC showing different stages of the experimental procedure to retrieve samples using a focussed ion beam for TEM imaging and electron diffraction. (1) Pt deposition. (2,5) Successful lamella extraction. (3,4) Failed lamella extractions. (inset) A schematic showing the orientation of the incoming electron beam in the TEM relative to the compression axis. The red circle indicates the boundary between the GC sample and the stainless-steel gasket.

Figure 2(a) is a TEM image (taken using a JEOL 2100F TEM operating at 200 kV) of uncompressed GC showing the tangled isotropic nanostructure consisting of curved graphitic stacks of up to ~10 layers. A TEM image from the recovered sample following compression to 35 GPa is shown in Fig. 2(c). This image shows a similar structure to that observed in the uncompressed case with the entanglement of graphitic sheets still present. After compression to 35 GPa the characteristic GC nanostructure remains intact, consistent with previous observations [15]. However, a significant change in the nanostructure is evident in the TEM image from the recovered sample following compression to 45 GPa as shown in Fig. 2(e). This image shows that some of the curved graphitic sheets are destroyed and are fully replaced with small graphitic crystallites with significant short-range order.

The observed changes in the nanostructure were further analysed by electron diffraction. Diffraction patterns are shown in Fig. 2 for (b) uncompressed GC, (d) GC after compression to 35 GPa, and (f) GC after compression to 45 GPa. The diffraction pattern of uncompressed GC shows the rings typical of nanocrystalline graphite exhibiting strong {002}, {100}, and {110} reflections. It should be noted that for the uncompressed GC sample each diffraction ring has a uniform distribution of intensity, proving that the nanostructure has random orientation. Figure 2(d) shows that after compression to 35 GPa, the diffraction rings still have uniform intensity, although there is some evidence for increased structural order from the sharpening of the diffraction rings. However, the diffraction pattern of the sample after compression to 45 GPa shows a highly non-uniform distribution of intensity. Therefore, the sample undergoes a significant permanent structural change. The graphitic planes are now preferentially oriented and aligned perpendicular to the direction of compression. This new preferred

orientation minimizes the elastic strain energy as a result of the strongly anisotropic elastic moduli of graphite [27,28]. A similar phenomenon has previously been described for pure graphite and is used to create highly oriented pyrolytic graphite under uniaxial stress conditions and high temperatures [29]. The development of nanocrystalline graphite following compression to 45 GPa is indicative of a loss of the superelastic property of GC, as the isotropic topology of the original sheet nanostructure has been destroyed and replaced with graphite that does not exhibit the superelastic property [30,31].
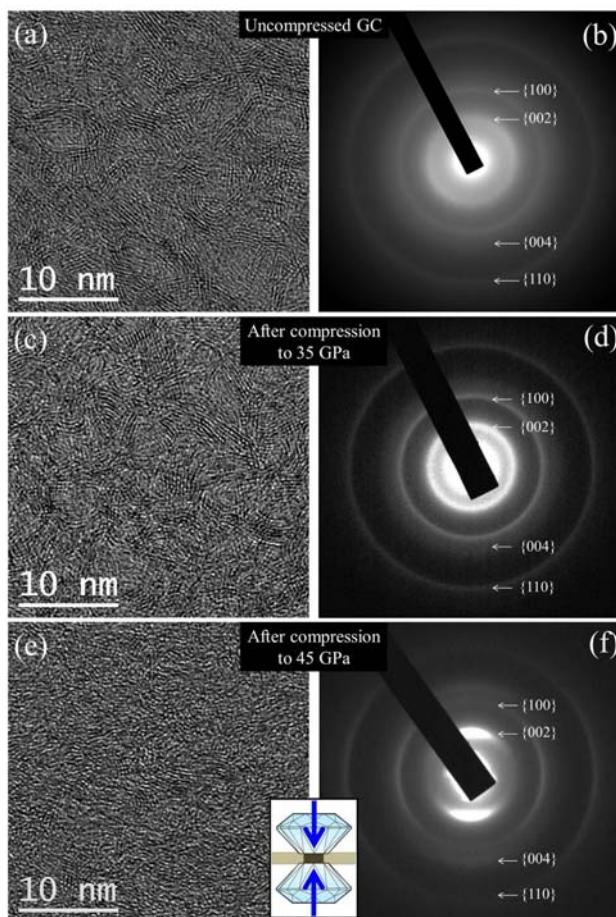

Figure 2: TEM images and selected area diffraction patterns (indexed to graphite) of (a,b) uncompressed GC, (c,d) the sample recovered from 35 GPa and (e,f) the sample recovered from 45 GPa. (inset) the compression axis of the DAC is indicated by the blue arrows.

Direct evidence for the loss of the superelastic properties comes from electron energy loss spectroscopy (EELS) density measurements (Gatan Tridiem Imaging Filter fitted to a JEOL 2100F TEM operating at 80 kV) which are known to be a sensitive measure of both the bonding and density [32]. The position of the plasmon peak in the low loss EELS spectra [Supplementary Fig. S1(a)] is proportional to the density of free electrons and therefore can be used to estimate the local microscopic density [33] of the uncompressed GC, giving a value of 1.62 g/cc. This value is lower than the density of graphite (2.27 g/cc), but it is higher than the manufacturer's specified macroscopic density of 1.42 g/cc. The macroscopic density includes the contribution from voids and thus differs from the EELS density [34]. The density of the recovered GC samples as a function of pressure is shown in Fig. 3. It reveals no significant change in microscopic density for samples compressed up to

35 GPa, but a significant permanent increase in microscopic density to 1.86 g/cc occurs for samples compressed to 45 GPa and above. A nanostructure consisting of stacked graphitic regions [Fig. 2(e,f)] is more efficiently packed than the tangled GC nanostructure leading to this increase in microscopic density.

To investigate bonding changes in the material, the carbon K-edge EELS of the uncompressed and recovered GC materials was measured [Supplementary Fig S1(b)]. All spectra exhibit a strong 1s to π^* peak at 285 eV consistent with a dominance of sp^2 bonding [32]. The sp^2 fractions were calculated from the carbon K-edge spectra using a method similar to that described by Berger [35]. Care must be taken when calculating sp^2 fractions of the recovered samples, as preferred orientation is known to strongly influence the intensity of the 1s to π^* peak [36]. This influence of preferred orientation can be accounted for by performing EELS measurements at the so-called 'magic angle' conditions where the intensity of the 1s to π^* peak does not vary with orientation of the graphitic crystallites relative to the incident beam [37]. This magic angle EELS (performed using specific electron beam convergence and spectrometer collection angles) enables the sp^2 to sp^3 bonding ratio to be measured even in the highly oriented sample recovered after compression to 45 GPa. At least four measurements were taken on each sample and the results are plotted in Fig. 3. The results show that the uncompressed GC has a sp^2 bonding fraction of 95±2% and a small fraction of sp^3 bonds. The fraction of sp^2 to sp^3 bonding does not change for samples compressed up to 35 GPa. For samples recovered after compression to 45 GPa and above, there is an increase in the sp^2 bonding fraction to ~100%. This result suggests that when raised to the threshold pressure of 45 GPa, any pre-existing sp^3 bonds are destroyed either on loading or on pressure release.

Raman spectra were collected (using a Renishaw InVia micro-Raman Spectrometer, equipped with a 532 nm excitation laser) from each of the recovered GC samples (Supplementary Fig. S2). The Raman peak positions do not change substantially from reported peak positions [38] after compression, however the relative integrated intensities do show a sharp discontinuity between 35 and 45 GPa (fitted peak parameters in Supplementary Table S1). The relative integrated intensities can also be used to determine the average in-plane graphitic crystallite sizes, L_a [39]. Figure 3 shows that L_a of the uncompressed GC is 10.3 nm, and decreases to 8.1 nm between 35 GPa and 45 GPa, supporting our observations of significant changes in nanostructure observed in the TEM results.
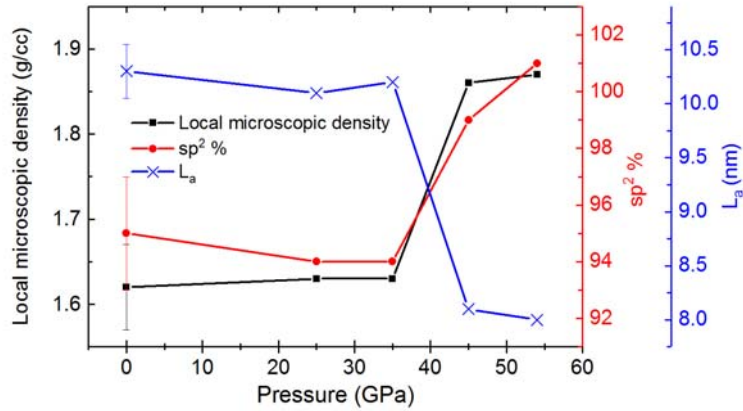
Figure 3: Local microscopic density (black squares), sp^2 fraction (red circles) obtained from EELS, and average in-plane crystallite size L$_a$ (blue crosses) obtained from Raman spectroscopy. Interestingly, the Raman spectra were better fitted with two peaks in the f-band region. However, the physical origin of these peaks remains unknown.

To assist in the interpretation of our experimental data, atomistic simulations of uniaxial compression and decompression were performed using the LAMMPS molecular dynamics package [40] with interactions described by the EDIP carbon interatomic potential [41]. The starting point of the simulations was a 1.5 g/cc structure [Fig. 4(a)] containing 32,768 atoms, generated using a liquid quench and annealing methodology [42]. The starting structure contains graphene layers with different orientations, characteristic of GC, and is highly sp^2 bonded. Upon compression, the graphene layers gradually align perpendicular to the applied stress [Fig. 4(b)]. At higher pressures, cross-linking sp^3 bonds form between layers, increasing the sp^3 fraction substantially [Fig. 4(d)]. Structures compressed to 10, 25, 35, 45 and 56 GPa were fully decompressed using the same strain rate as the compression, in combination with annealing of the decompressed structure at 3500 K to activate atomic rearrangement. At low maximum compression (e.g. to 10 GPa) the structure recovers its original bonding architecture upon decompression, although the details of the bonding has been altered in some regions [Fig. 4(c)]. These simulations are consistent with our experimental data for pressures less than 35 GPa and are consistent with the superelastic behaviour of GC. At higher pressure (e.g. 45 GPa), the decompressed structure has a similar sp^2 fraction to the original structure, however the graphitic layers have preferentially re-aligned perpendicular to the applied stress direction [Fig. 4(d,e)]. The development of preferred orientation of the graphitic layers is consistent with our experimental observations at similar pressures. Additionally, the structures that have been compressed to pressures above ~35 GPa do not recover their original density upon decompression [black circles in Fig. 4(f)], but have a permanently increased density as seen experimentally (Fig. 3). Figure 4(f) also shows the sp^3 fraction of the compressed phase (blue squares), displaying a transition at around 35 GPa, to a structure with a high sp^3 fraction. This high sp^3 structure is unstable and reverts to a high sp^2 fraction structure upon pressure release, as shown in the Fig. 4(d,e).

6
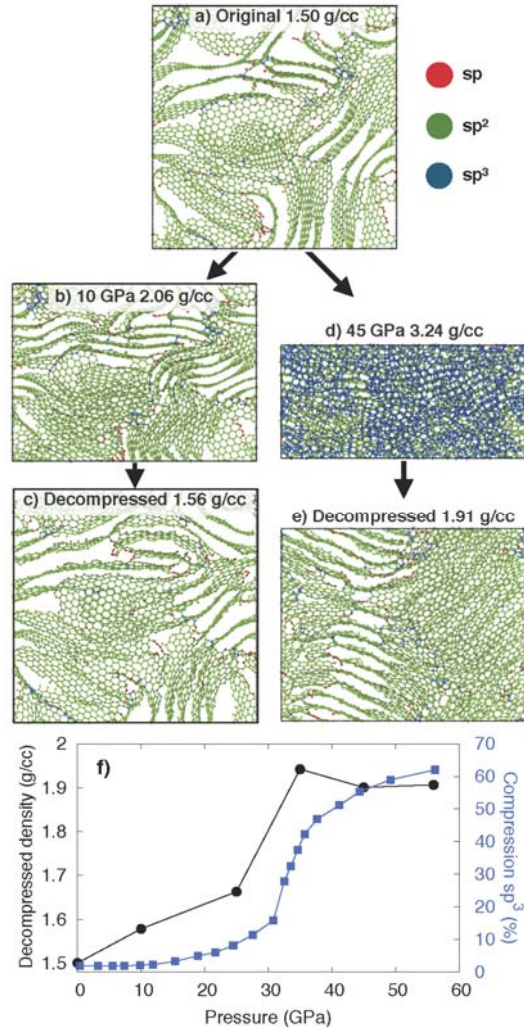
Figure 4: (a-e) Snapshots of compression/decompression simulations of GC, showing 2 nm thick slabs. Red, green, blue circles denote sp, sp^2, sp^3 bonding, respectively. (a) Original GC structure; (b) GC compressed to 10 GPa; (c) Structure (b) decompressed to zero-pressure; (d) GC compressed to 45 GPa; (e) Structure (d) decompressed to zero-pressure; (f) Density of simulated structures after decompression (black circles) and their sp^3 fraction while under pressure (blue squares) as a function of the maximum pressure experienced.

Following recovery after compression up to 35 GPa, both experiment and simulation show that the isotropic nanostructure of GC is retained. This demonstrates that the GC nanostructure, which consists of extremely strong and tangled graphene sheets, is highly resilient to compression. The superelastic property of GC is the manifestation of this resilience.

At pressures of 45 GPa and above, our simulations show that a majority sp^3 phase is formed that is unstable when pressure is released. Several other theoretical studies have also predicted the formation of exotic unstable sp^3 rich phases at high pressures [19-23]. These findings from theory are consistent with the experimental work of Lin that showed the sp^3 bonds formed by loading GC to pressures up to 44 GPa reverted to sp^2 bonds on pressure release [16]. Moreover, it has recently been reported that an exotic sp^3 phase, known as M-carbon, has been experimentally observed during the room temperature compression of graphite at ~40 GPa [43], which spontaneously transformed back to sp^2 bonded

graphite on pressure release. We propose that a similar high pressure sp^3 rich phase is formed in our GC at pressure of 45 GPa and above. This sp^3 structure is unstable at ambient. At high pressure, the tangled GC nanostructure including any fullerene-like elements is destroyed as the dominant bonding changes from sp^2 to sp^3. The transformation to a sp^3 rich phase and then down to a fully sp^2 bonded phase would explain why on pressure release, the sample does not recover its original isotropic tangled sheet-like structure but instead shows permanent preferred orientation of the newly formed sp^2 bonded graphite. The graphite is oriented [Fig. 2(f)] reflecting its formation in a stress field with a strong uniaxial component. Since the formation of extensive preferred orientation of the graphitic layers is essentially graphitization, we propose that compression of GC to 45 GPa and above causes a loss of its superelastic properties since graphite is not superelastic.

In summary, we have used TEM imaging, electron diffraction, EELS, Raman spectroscopy and atomistic modelling to understand the superelastic and non-graphitizing characteristics of GC as it is compressed at room temperature. After loading up to 35 GPa, the recovered material is found to retain its tangled nanostructure, including its minority content of sp^3 bonding (~5%). In contrast, the samples recovered after compression to over 45 GPa contains a negligible sp^3 bonding content (~0%). Pressures above this threshold cause the tangled sheet structure to align as the sheets come closer together, and the modelling shows that new sp^3 bonds form but are unstable at ambient. Experimental results also show permanent densification and the formation of oriented graphite layers in GC subjected to such pressures. Accordingly, this 45 GPa threshold represents the ultimate limit to the non-graphitizing and superelastic properties of GC and this work provides valuable insight into the transition pathway of pressure-induced structural and bonding changes in GC.

References:

[1]   K. A. H. Al Mahmud, M. A. Kalam, H. H. Masjuki, H. M. Mobarak, and N. W. M. Zulkifli, Crit. Rev. Solid State Mater. Sci. **40**, 2 (2014).
[2]   C. A. Charitidis, Int. J. Refract. Met. Hard Mater. **28**, 1 (2010).
[3]   R. Sengupta, M. Bhattacharya, S. Bandyopadhyay, and A. K. Bhowmick, Prog. Polym. Sci. **36**, 5 (2011).
[4]   N. Iwashita, M. V. Swain, J. S. Field, N. Ohta, and S. Bitoh, Carbon. **39**, 10 (2001).
[5]   G. M. Jenkins and K. Kawamura, Nature **231**, 5299 (1971).
[6]   F. C. Cowlard and J. C. Lewis, J. Mater. Sci. **2**, 6 (1967).
[7]   Z. Zhang, R. Brydson, Z. Aslam, S. Reddy, A. Brown, A. Westwood, and B. Rand, Carbon. **49**, 15 (2011).
[8]   A. Aherwar, A. K Singh, and A. Patnaik, AIMS Bioeng. **3**, 1 (2015).
[9]   J. Myalski and J. Śleziona, J. Mater. Process. Technol. **175**, 1-3 (2006).
[10]   C. Blanco, J. Bermejo, H. Marsh, and R. Menendez, Wear **213**, 1-2 (1997).
[11]   P. J. F. Harris, Philos. Mag. **84**, 29 (2004).
[12]   T. B. Shiell, D. G. McCulloch, J. E. Bradby, B. Haberl, R. Boehler, and D. R. McKenzie, Sci. Rep. **6**, 37232 (2016).
[13]   Y. Hishiyama, M. Inagaki, S. Kimura, and S. Yamada, Carbon. **12**, 3 (1974).
[14]   R. R. Saxena and R. H. Bragg, Carbon. **16**, 5 (1978).

[15] Z. Zhao, E. F. Wang, H. Yan, Y. Kono, B. Wen, L. Bai, F. Shi, J. Zhang, C. Kenney-Benson, C. Park, Y. Wang, and G. Shen, Nat. Commun. **6**, 6212 (2015).

[16] Y. Lin, L. Zhang, H. K. Mao, P. Chow, Y. Xiao, M. Baldini, J. Shu, and W. L. Mao, Phys. Rev. Lett. **107**, 17 (2011).

[17] N. A. Solopova, N. Dubrovinskaia, and L. Dubrovinsky, Appl. Phys. Lett. **102**, 12 (2013).

[18] M. Yao, J. Xiao, X. Fan, R. Liu, and B. Liu, Appl. Phys. Lett. **104**, 021916 (2014).

[19] F. J. Ribeiro, P. Tangney, S. G. Louie, and M. L. Cohen, Phys. Rev. B - Condens. Matter Mater. Phys. **72**, 214109 (2005).

[20] M. Amsler, J. A. Flores-Livas, L. Lehtovaara, F. Balima, S. A. Ghasemi, D. MacHon, S. Pailhes, A. Willand, D. Caliste, S. Botti, A. San Miguel, S. Goedecker, and M. A. L. Marques, Phys. Rev. Lett. **108**, 065501 (2012).

[21] K. Umemoto, R. M. Wentzcovitch, S. Saito, and T. Miyake, Phys. Rev. Lett. **104**, 125504 (2010).

[22] J. T. Wang, C. Chen, and Y. Kawazoe, Phys. Rev. B - Condens. Matter Mater. Phys. **85**, 033410 (2012).

[23] Q. Li, Y. Ma, A. R. Oganov, H. Wang, H. Wang, Y. Xu, T. Cui, H. K. Mao, and G. Zou, Phys. Rev. Lett. **102**, 175506 (2009).

[24] M. Hu, J. He, Z. Zhao, T. A. Strobel, W. Hu, D. Yu, H. Sun, L. Liu, Z. Li, M. Ma, Y. Kono, J. Shu, H. Mao, Y. Fei, G. Shen, Y. Wang, S. J. Juhl, J. Y. Huang, Z. Liu, B. Xu, and Y. Tian, Sci. Adv. **3**, 6 (2017).

[25] Z. Zeng, L. Yang, Q. Zeng, H. Lou, H. Sheng, J. Wen, D. J. Miller, Y. Meng, W. Yang, W. L. Mao, and H. K. Mao, Nat. Commun. **8**, 322 (2017).

[26] H. K. Mao, J. Xu, and P. M. Bell, J. Geophys. Res. **91**, B5 (1986).

[27] D. R. McKenzie, D. Muller, and B. A. Pailthorpe, Phys. Rev. Lett. **67**, 6 (1991).

[28] M. B. Taylor, D. W. M. Lau, J. G. Partridge, D. G. McCulloch, N. A. Marks, E. H. T. Teo, and D. R. McKenzie, J. Phys. Condens. Matter **21**, 225003 (2009).

[29] L. C. F. Blackman and A. R. Ubbelohde, Proc. R. Soc. A Math. Phys. Eng. Sci. **266**, 1324 (1962).

[30] J. S. Field and M. V. Swain, Carbon. **34**, 11 (1996).

[31] J. Skinner and N. Gane, Philos. Mag. **28**, 4 (1973).

[32] R. F. Egerton, *Electron Energy-Loss Spectroscopy in the Electron Microscope* (Springer Science & Business Media, 2011).

[33] J. T. Titantah and D. Lamoen, Phys. Rev. B - Condens. Matter Mater. Phys. **70**, 033101 (2004).

[34] J. Schwan, S. Ulrich, T. Theel, H. Roth, H. Ehrhardt, P. Becker, and S. R. P. Silva, J. Appl. Phys. **82**, 12 (1997).

[35] S. D. Berger, D. R. McKenzie, and P. J. Martin, Philos. Mag. Lett. **57**, 6 (1988).

[36] N. Browning, J. Yuan, and L. Brown, Ultramicroscopy **38**, 3-4 (1991).

[37] H. Daniels, A. Brown, A. Scott, T. Nichells, B. Rand, and R. Brydson, Ultramicroscopy **96**, 3-4 (2003).

[38] A. C. Ferrari and J. Robertson, Philos. Trans. Math. Phys. Eng. Sci. **362**, 1824 (2004).

[39] L. G. Cançado, K. Takai, T. Enoki, M. Endo, Y. A. Kim, H. Mizusaki, A. Jorio, L. N. Coelho, R. Magalhães-Paniago, and M. A. Pimenta, Appl. Phys. Lett. **88**, 163106 (2006).

[40] S. Plimpton, J. Comput. Phys. **117**, 1 (1995).

[41] N. A. Marks, Phys. Rev. B. **63**, 035401 (2000).

[42] C. de Tomas, I. Suarez-Martinez, and N. A. Marks, Carbon. **109**, p681-693 (2016).

[43] Y. Wang, J. E. Panzik, B. Kiefer, and K. K. M. Lee, Sci. Rep. **2**, 520 (2012).